



# Thermophysical properties of n-alkyl-ammonium nitrate ionic liquids (n = 2,3,4) pure and water saturated for energy applications

J. J. Parajó<sup>1,2</sup> · P. Vallet<sup>1</sup> · M. J. G. Guimarey<sup>1,3</sup> · A. Santiago<sup>1</sup> · T. Teijera<sup>1</sup> · A. Amigo<sup>4</sup> · L. M. Varela<sup>1</sup> · J. Salgado<sup>1</sup> · M. Villanueva<sup>1</sup>

Received: 2 August 2022 / Accepted: 16 April 2023 / Published online: 12 May 2023  
© The Author(s) 2023

## Abstract

Phase transition temperatures of three ionic liquids (ILs) with ammonium cations of different alkyl chain length and nitrate common anion were determined in this paper by differential scanning calorimetry. Thermal stability of these ILs in air and nitrogen atmosphere and the maximum operation temperatures of the compounds were also studied using a thermogravimetric analyser. Furthermore, thermophysical properties as density, viscosity, thermal conductivity, and heat capacity against temperature of these pure ionic liquids were determined and compared with the corresponding values for water saturated samples. For this purpose, different techniques were employed: for density and viscosity a rotational automated viscosimeter; for thermal conductivity measurements a thermal conductimeter that follows the transient hot-wire method; and for heat capacity measurements a microdifferential scanning calorimeter. Different behaviours were observed depending on the analysed thermophysical properties. In case of dried samples, density and thermal conductivity decrease with alkyl chain; for saturated samples, same tendency is observed for density but is the opposite in case of thermal conductivity. Isobaric specific heat and viscosity increase with alkyl chain length in case of dried samples; for saturated samples same tendency is observed for the viscosity, whereas the tendency is the contrary in case of isobaric specific heat.

**Keywords** Ionic liquids · Water content · Transport properties

## Introduction

Ionic liquids (ILs) are composed by an organic cation and an inorganic/organic anion and usually are defined as molten salts with melting point below 100 °C. The first ionic liquid, ethylammonium nitrate (EAN), was synthesized by Paul Walden more than a hundred years ago. Although EAN has been widely studied, some important aspects and properties are not deeply analysed and discussed for this IL and others alkyl-ammonium cation family ILs [1]. Alkyl-ammonium nitrate ILs are included in the subcategory of protic ILs (PILs), which are usually prepared by proton transfer from acid to organic bases [2, 3]. Hence, they present the advantages of being cheaper and easier to synthesize and more harmless compared with the aprotic ILs (APILs) but with weakness of the water affinity and shorter thermal stability than aprotic [4–7].

Due to their tuneable properties [5, 8–13], this new family of green solvents has been recognized as a clear and viable alternative in a huge variety of industrial processes in which the use of aqueous or organic-based media

---

J. J. Parajó and P. Vallet have Contributed equally to this work.

✉ J. Salgado  
j.salgado.carballo@usc.es

✉ M. Villanueva  
maria.villanueva@usc.es

<sup>1</sup> Grupo de Nanomateriais, Fotónica e Materia Branda, Departamentos de Física Aplicada y Física de Partículas, Universidade de Santiago de Compostela, Campus Vida S/N, 15782 Santiago de Compostela, Spain

<sup>2</sup> Departamento de Química e Bioquímica, CIQUP Centro de Investigação em Química da Universidade do Porto, Universidade do Porto, Rua do Campo Alegre, 4169-007 Porto, Portugal

<sup>3</sup> Department of Design and Engineering, Faculty of Science and Technology, Bournemouth University, Poole, Dorset BH12 5BB, UK

<sup>4</sup> Grupo de Propiedades Termofísicas e Superficiais de Líquidos, Departamento de Física Aplicada, Universidade de Santiago de Compostela, Campus Vida S/N, 15782 Santiago de Compostela, Spain

is not convenient. These compounds have represented a revolution in the field of solvents for advanced devices, for synthesis and catalysis or thermal fluids of high liquid range and enormous stability. A large set of ILs meet all the requirements to be classified as smart materials, since they usually present great variations of their properties with the modification of external variables such as water content, temperature, and electric field. Therefore, these compounds, pure or in mixtures with other substances (salts, solvents, etc.), can be used, for example, in electrochemistry purposes [14, 15] as elements of fuel cell electrode reactions and electrolytes for next generation batteries. The study of mixtures of these systems with cosolvents and inorganic salts of electrochemical interest (Li, Na, Mg, Ca, Al) [16] or transition metals or rare earth salts for their magnetic or optical properties—thermochromism and luminescence—has undergone a strong development during last years [17].

ILs have also been considered as candidates to replace conventional heat transfer fluids (HTFs), a heat transporter from a heat source to another heat demander as, for example, water, silicone polymers, synthetic fluids derived from mineral oils, benzenes or fluorocarbon designed to provide a precise control of temperature with applicability in solar collectors and refrigerator systems, among others [8, 18–20]. Three categories have been defined for the HTFs regarding their temperature range operation: low temperature (up to 290 °C), medium temperature (290–590 °C) or high temperature (more than 590 °C) HTFs [21].

Other interesting application of ILs in which different research groups have worked in recent years is as absorbents in absorption heat pumps with water or alcohol as refrigerants [8, 12, 22, 23]. The advantage of absorption systems against compression systems is the possibility of recovering residual heat or be powered by solar energy for their operation, instead of use electric power for mechanical compressors [12, 23]. The commercial absorption systems present problems of corrosion, crystallization, volatility or toxicity with the current (refrigerant/absorbent) working pairs, H<sub>2</sub>O/LiBr or NH<sub>3</sub>/H<sub>2</sub>O. New working pairs with ILs can solve or minimize these problems.

In summary, among other applications of ILs, the energy harvesting, transport and storage are subject of the highest scientific relevance. Hence, thermophysical characterization, such as thermal conductivity, heat capacity, density and viscosity, must be performed before an IL can be chosen as a smart material in these energetic applications.

It is important to note, as it is well known, that among the previously mentioned properties, ILs usually are hygroscopic and highly viscous, which for most authors is a disadvantage. But this high hygroscopicity makes them ideal candidates for moisture detection due to the huge variation of their electrical conductivity, and furthermore, the addition of

a molecular cosolvent like water (or carbonates) can reduce the viscosity [8, 22].

Also, it is well known that these protic ILs are nanostructured liquids with separated polar and apolar regions on the bulk, with the charge distributed in a large molecular volume with feeble electrostatic interactions and important H-bonds network [24, 25]. Although these ILs are the first to have been synthesized, most of their thermal and transport properties, essential for these applications, are unknown; only, Bouzón-Capelo et al. [26] present values of density, surface tension, viscosity and electrical conductivity for EAN, propylammonium nitrate (PAN) and butylammonium nitrate (BAN) and Ausín et al. [27] analyse the influence of small quantities of water in EAN and PAN on the density, viscosity, electrical conductivity, refractive index and surface tension.

The aim of this work is to characterize relevant thermophysical properties of these ILs, completing the results of Bouzón-Capelo et al. and those of Ausín et al. [26, 27] reporting the liquid range window, heat capacity, density, viscosity and thermal conductivity, of pure and dried alkylammonium ionic liquids EAN, PAN and BAN and to compare these results with the obtained for the same water saturated ionic liquids in terms of the mesoscale structure.

## Materials and methods

### Chemicals

Three protic ionic liquids, ammonium based with different alkyl chain length and common anion, nitrate, provided by IoLiTec were studied in this work: EAN, PAN and BAN. Identification names, abbreviations, CAS numbers, chemical structures, molecular mass and mass fraction purities are presented in Table 1.

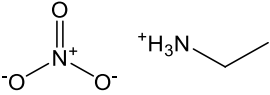
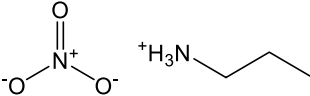
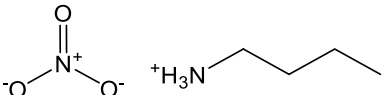
Samples were previously purified by a vacuum pump during at least 24 h before the thermophysical characterization, being water contents below 100 ppm in all cases (determined by Karl Fischer titration). To analyse the influence of environmental water on the thermophysical properties, samples of the three ILs were exposed in an open vial to ambient conditions of humidity and temperature until saturated level of humidity was attained.

### Experimental

#### Phase transition determination

A differential scanning calorimeter DSC Q100 from TA Instruments was used to determine the different phase transitions experimented by the pure ILs during heating and cooling cycles. Samples, without further purification, were

**Table 1** Structure, identification, molar mass and mass fraction purity of selected ILs

Name	Abbreviation CAS number	Chemical structure	Molecular mass/g mol <sup>-1</sup>	Mass fraction purity
Ethylammonium nitrate	EAN C <sub>2</sub> H <sub>8</sub> N <sub>2</sub> O <sub>3</sub> 22,113-86-6		108.10	> 97
Propylammonium nitrate	PAN C <sub>3</sub> H <sub>10</sub> N <sub>2</sub> O <sub>3</sub> 22,113-88-8		122.12	> 97
Butylammonium nitrate	BAN C <sub>4</sub> H <sub>12</sub> N <sub>2</sub> O <sub>3</sub> 58,888-50-9		136.15	> 97

placed in a 40-mL hermetically sealed aluminium pan with a pinhole at the top of the cover. Each sample (3–5 mg) was subjected to four ramps, two in cooling and two in heating mode, with an isothermal step between them: (a) heating from (25 to 120) °C at 10 °C min<sup>-1</sup>, (b) isothermal step at 120 °C during 45 min to remove impurities and to erase the thermal history of the sample, (c) cooling from (120 to –85) °C at 5 °C min<sup>-1</sup>, (d) isothermal step at –85 °C during 5 min and (e) heating from (–85 to 100) °C at 10 °C min<sup>-1</sup> and (f) cooling from (100 to –85) °C at 5 °C min<sup>-1</sup>. Transitions temperatures were determined from the DSC curves, as the onset points of the different peaks, during the reheating and re-cooling steps. Temperature and heat of melting of indium were used for calibration. [15, 28]

### Thermogravimetric analysis

Thermogravimetric analysis has been performed to study the thermal stability of the BAN and PAN ILs and to compare it to the previously obtained results for thermal stability of EAN [15]. Dynamic mode was employed to analyse the short-term thermal stability under dry air and N<sub>2</sub> atmospheres. Dynamic scans were performed from (50 to 800) °C with a heating rate of 10 °C min<sup>-1</sup> and a purge gas flow of 20 cm<sup>3</sup> min<sup>-1</sup>. Samples of 3–5 mg were placed in an open platinum pan. Each analysis was performed three times. To determine the long-term thermal stability, isothermal analysis under N<sub>2</sub> atmosphere at temperatures lower to  $t_{\text{onset}}$  obtained in dynamic scans was done. In previous papers [7, 10, 28] more details about the methodology of this isothermal study are included. It was previously stated that water content does not influence on this analysis [29].

### Density

Density of the three pure ILs and their saturated forms at atmospheric pressure were measured from (288.15 to

368.15) K using a rotational automated Anton Paar Stabinger SVM3000. This apparatus [30] is equipped with a vibrating tube and permits measurements of the densities with an uncertainty of 0.0005 g cm<sup>-3</sup>. The temperature of the cell is controlled through an integrated thermostat with cascaded Peltier elements and measured with a Pt100 thermometer with an uncertainty of 0.02 K. This device has been described widely in previous papers [22, 31].

### Heat capacity

Specific heat capacities were obtained using the isothermal step method with a Micro DSCIII differential scanning calorimeter from Setaram, France. Calibration was performed using a Joule effect calibration vessel (Setaram) and checked using n-decane and squalane (Sigma-Aldrich 99%) as heat capacity standards [32]. Background noise of the Micro DSCIII was less than 3 μW. Dynamic scans of samples of around 0.8 mL were performed at a heating rate of 0.25 K min<sup>-1</sup> in the temperature interval (293.15–348.15) K. Squalane was used as the reference fluid to determine the heat capacity values due to the similar values of heat flow and to the high precision of the available literature data [32]. The experimental technique and procedure has been deeply previously described [33, 34], and the standard uncertainty in C<sub>p</sub> experimental values is estimated to be 0.002 J g<sup>-1</sup> K<sup>-1</sup>.

### Thermal conductivity

Thermal conductivity data were collected using a TEMPOS Thermal Properties Analyser from METER Group. The transient hot-wire method is the principle of measurement of this equipment [35]. The meter was a thermal probe KS-3 (1.3 mm diameter, 60 mm length) that contains a heater and a temperature sensor inside. This sensor has an accuracy of 10% in a range of 0.02–2.00 W m<sup>-1</sup> K<sup>-1</sup> for thermal conductivity and 0.001 K for temperature measurements. A sample

volume of 10 cm<sup>3</sup> approximately must be introduced in a sealed glass vial. The probe must be vertically placed into the sample to minimize convective effects. Once the sample is inside the vial, this is fully immersed in a temperature-controlled water bath (PolyScience). Thermal conductivity measurements were repeated 5 times for each temperature. A delay of at least 15 min was maintained to ensure complete equilibration between each pair of data determination. One minute reading time is necessary for each of the five measurements. Thermal conductivities were measured over the temperature range from (293.15 to 323.15) K in 5 K steps.

This device does not require calibration, only periodic verification of the sensor. This verification was done by measuring a known thermal conductivity standard (glycerin) [36].

### Viscosity

The dynamic viscosities of the three dried and saturated ILs were measured under air atmosphere using two methodologies. Firstly, to verify the Newtonian regime, a rheometer TA Instruments AR2000 stress control, with a Peltier cooling device that controls the temperature value was used. A geometry of cone and plate with a diameter of 60 mm, an angle of 1° and a truncation of 28 μm was employed. Both the sample and the geometry were covered with a lid to avoid the exchange of atmospheric water with the environment. From this rheology studies, the viscosity values were obtained with temperature sweep stepped tests with a temperature increment of 5 K and 3 min of equilibration time before each measurement, 10 Pa of oscillatory stress (selected in a preliminary study in the linear viscoelastic region of the liquids) and 1 Hz of frequency. The temperature range of the experiment was (283.15–338.15) K.

The second methodology used is the rotational automated viscometer Anton Paar Stabinger SVM3000, also used to density determinations. Dynamic and kinematic viscosities from (278.15 to 378.15) K, in a viscosity range from 0.2 mPa s to 20 Pa s with an experimental expanded uncertainty of 1% [30] were measured [37, 38]. Comparison between dynamic viscosities obtained from both methods was performed.

### Effects of the absorption of the environmental water on the thermophysical properties

With the aim to determine the changes of thermophysical properties due to water absorption capacity of these ILs, samples of EAN, BAN and PAN were exposed to the atmosphere for several days in an open recipient at ambient temperature and humidity until saturation. Density, heat capacity, viscosity and thermal conductivity of these samples were determined using the same methodologies indicated above.

The water content of the ILs was measured by gravimetry. As it was expected, the three ILs undergo a high increase of their masses due to the high-water affinity of PILs. It has also been observed that the equilibrium was attained after one week, but they were exposed 20 days to check if this equilibrium was stable, confirming that water uptake oscillated depending on the relative humidity of the environment, which is extremely sensible to weather changes.

Mass and mole fractions of water after 20 days of exposure of every IL are shown in Table 2. Water mole fraction was calculated as:

$$x_{\text{H}_2\text{O}} = \frac{n_{\text{H}_2\text{O}}}{n_{\text{H}_2\text{O}} + n_{\text{IL}}} \quad (1)$$

Molecular mass of saturated samples ( $M_{\text{mss}}$ ) was calculated as:

$$M_{\text{mss}} = M_{\text{mIL}} + \gamma M_{\text{mH}_2\text{O}} \quad (2)$$

$$\gamma = \frac{\chi_{\text{H}_2\text{O}}}{\chi_{\text{IL}}} \quad (3)$$

where  $\gamma$  is the relation between the mole fraction of water and the IL.

As it can be seen, the lower the molar mass (or the alkyl chain length) of the IL, the greater the water uptake, as it could be expected since the hydrophilicity decreases with the chain length [39].

## Results and discussion

### Liquid range

For the correct determination of the liquid range, defined as the range between melting and thermal degradation temperatures, impurities (e.g. water content) must be removed [28], especially for thermal transition at low temperatures. For this purpose, an isothermal step was introduced in the DSC routine, as it was previously pointed out. The determination of liquid range has only been done for the dried samples since

**Table 2** Water content of saturated EAN, PAN and BAN samples in % in mass of dry IL, corresponding mole fraction of water and molecular mass of the mixture

IL	Water uptake/%	Water mole fraction	Molecular mass/g mol <sup>-1</sup>
EAN	22.5	0.574	132.41
PAN	15.2	0.507	140.7
BAN	10.2	0.435	150.0

in previous reports it has been concluded that water does not significantly affect the liquid window [28, 40].

### DSC phase transition analysis

The DSC curves corresponding to the last heating and cooling steps performed at  $5\text{ }^{\circ}\text{C min}^{-1}$  are shown in Fig. 1. To better visualize the thermal transitions, the curves were presented in a narrower range temperature than the experimental one.

It can be seen in Fig. 1a and b that EAN presents a cold-cold transition at  $-44\text{ }^{\circ}\text{C}$  followed by a melting at  $12\text{ }^{\circ}\text{C}$  in the heating ramp, and a freezing point at  $-27\text{ }^{\circ}\text{C}$  in the cooling ramp, as previously reported [15]. In the case of PAN, no cold-cold transition is observed, and melting and

freezing transitions were detected at  $5$  and  $-28\text{ }^{\circ}\text{C}$ , in heating and cooling ramps respectively. BAN is solid at room temperature and this behaviour is observed on his thermal transitions; a cold-cold transition and a melting at  $-38$  and  $40\text{ }^{\circ}\text{C}$  were observed in the heating ramp, respectively, and a freezing point is detected at  $-6\text{ }^{\circ}\text{C}$ .

Table 3 summarizes the thermal transitions obtained from DSC curves of the three ILs in cooling and heating ramps. Results for EAN have been previously reported [15]. Nevertheless, they are shown in this table for a better comparison. The three ILs showed a crystalline behaviour, characterized by a freezing process (exothermic peak in cooling ramp) and a melting process (endothermic peak in heating ramp). Additionally, EAN seems to have more difficulties to crystallize due to the presence of a clear cold crystallization

**Fig. 1** DSC profile comparison on heating (a) and cooling (b) ramps for EAN (red circles), PAN (blue triangles) and BAN (green squares) PILs

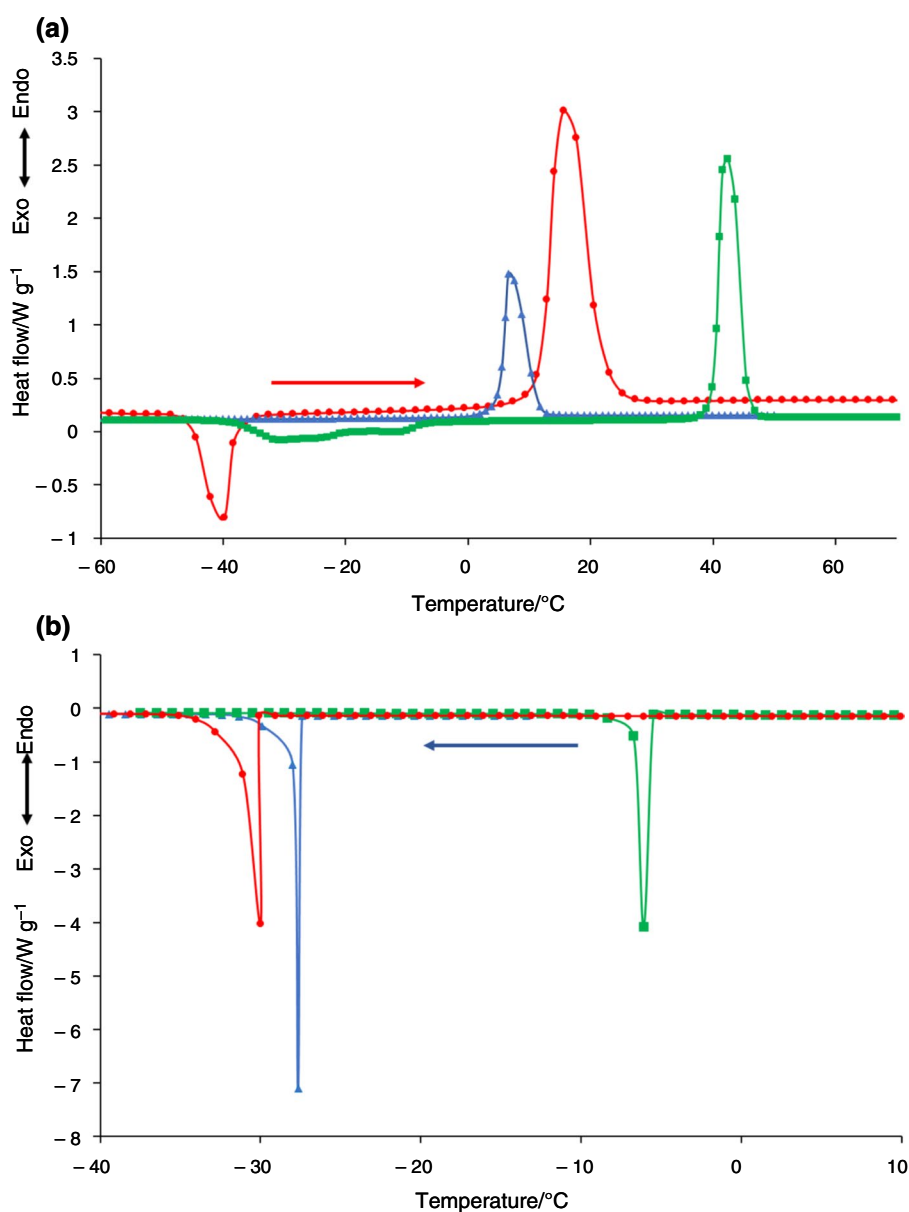


**Table 3** Temperature, enthalpy and entropy of melting per gram and per mol of sample ( $t_m$ ,  $\Delta H_m$  and  $\Delta S_m$ ), temperature and enthalpy of freezing per gram of sample ( $t_f$  and  $\Delta H_f$ ), and temperature and enthalpy of cold crystallization ( $t_{cc}$  and  $\Delta H_{cc}$ ) of the ILs

IL	$t_f/^\circ\text{C}$	$t_m/^\circ\text{C}$	$t_{cc}/^\circ\text{C}$	$\Delta H_{cc}/\text{J g}^{-1}$	$\Delta H_f/\text{J g}^{-1}$	$\Delta H_m/\text{J g}^{-1}$	$\Delta H_m/\text{kJ mol}^{-1}$	$\Delta S_m/\text{J g}^{-1} \text{K}^{-1}$	$\Delta S_m/\text{J mol}^{-1} \text{K}^{-1}$
EAN [15]	-27	12	-44	30	76	122	13.2	0.43	46
PAN	-28	5	-	-	-	71	8.6	0.25	31
BAN	-6	40	-38	47	-	126	17.1	0.40	55

Experiments were performed under an atmospheric pressure of  $(1008 \pm 10)$  hPa and a relative humidity of  $(55 \pm 10)\%$

Expanded uncertainties are  $U(t) = 6^\circ\text{C}$  and  $U_f(\Delta H) = 4\%$  [0.95 level of confidence ( $k = 2$ )]

peak (exothermic in heating ramp), which is not so clear for PAN and BAN. Moreover, due to the fact that freezing temperatures are markedly lower than melting temperatures, a clear supercooling effect, typical in ILs [29, 41], has been observed for the three ILs.

Scarce bibliographic data can be found for these ILs, except for EAN, as we pointed out in our previous paper [15]. Results of Atkin and Warr [42] are in good agreement with our results of melting temperatures of EAN and PAN. Likewise, I. Vázquez Fernández in her Ph-D thesis [43] presents similar values for the melting point of the three ILs, but surprisingly the paper of Canongia et al. [44], which is an article originated from this Ph-D thesis, indicates a melting point of  $183^\circ\text{C}$  for BAN, far from our results, which is clearly a mistake, also taking into account that this paper shows different thermophysical properties associated to liquid state at  $40^\circ\text{C}$ .

PAN shows the lowest melting temperature and BAN the highest, seeming that the odd and even number of alkyl chain groups presents different behaviour, increasing the melting point with the length, although it must be corroborated with additional studies.

## Thermal stability

**Dynamic study.** TG and DTG curves of the three selected ILs in dynamic mode under air and nitrogen atmospheres can be seen in Figure S1 (see electronic supplementary

material, ESI). As with DSC study, thermal stability of EAN has been previously studied and reported [15] and here included for the comparison with PAN and BAN. All ILs show a unique step in thermogravimetric curve and a unique peak in DTG curve. Thermal stability parameters obtained from the curves of the three ILs are shown in Table 4. Onset and endset temperatures,  $t_{\text{onset}}$  and  $t_{\text{endset}}$ , respectively, as well as  $W_{\text{onset}}$ ,  $t_{10\%}$  and  $t_{\text{peak}}$ , were determined following the criterion indicated in previous works [4, 15]. No significant differences between the values of the onset temperature in the two atmospheres for this group of ammonium based ILs were observed. The difference between the onset temperatures in both atmospheres, which is within the conventional experimental error, states that there is no influence of the atmosphere in this type of results, indicating that an oxygen independent mechanism, such as evaporation, is the main mechanism for the loss of mass for these ILs [5, 15].

These ILs exhibit similar onset temperatures, as it can be expected, taking into account the strong influence of the anion on this property, although the alkyl chain length tends to slightly reduce the thermal stability, which is low compared to other aprotic ILs frequently studied, such as those containing [OTf] or [NTf<sub>2</sub>] anions, whose  $t_{\text{onset}}$  values fall around  $400^\circ\text{C}$  [45–47] that is, more than  $150^\circ\text{C}$  above the values of the three ILs here reported.

In the same way as for temperature of the thermal transitions, scarce previous references can be found in the literature and values are in relatively good agreement with

**Table 4** Onset and endset temperatures ( $t_{\text{onset}}$ ,  $t_{\text{endset}}$ ), temperature at 90% of remaining mass ( $t_{10\%}$ ), sample remaining mass (in %) at onset temperature ( $\text{Mass}_{\text{onset}}$ ) and temperature of the minimum of DTG ( $t_{\text{peak}}$ ) from the dynamic scans ( $10^\circ\text{C min}^{-1}$ ) in air and nitrogen atmospheres

IL	Atmosphere	$t_{\text{onset}}/^\circ\text{C}$	$t_{\text{endset}}/^\circ\text{C}$	$t_{10\%}/^\circ\text{C}$	$\text{Mass}_{\text{onset}}/\%$	$t_{\text{peak}}/^\circ\text{C}$	$\text{H}_2\text{O}/\%$
EAN [15]	air	245	262	235	76	257	5
	N <sub>2</sub>	248	265	240	73	260	9
PAN	air	241	258	218	70	255	2
	N <sub>2</sub>	244	259	223	72	255	2
BAN	air	231	248	231	88	242	2
	N <sub>2</sub>	235	247	230	83	244	2

Experiments were performed with  $(979 \pm 2)$  hPa of atmospheric pressure, and relative humidity of  $(75 \pm 16)\%$

our results despite the different criterion used to establish the onset temperature of this degradation process [43, 48].

**Isothermal study.** As it is well known [7], the onset temperature can be used as a parameter that characterizes the relative thermal stability (or short thermal stability), that is, to determine which IL within a certain group of ILs is the most or the least stable when exposed to high temperatures. Although it is not a definitive parameter to guarantee no degradation if this substance is exposed to this temperature. As it can be seen in Table 4, the mass loss that takes place at the onset temperature ( $100 - W_{\text{onset}}$ ) reaches values between 12 and 30%, which are too high to ensure the IL has not suffered appreciable degradation. In the same way, Figure S2 in ESI shows the mass loss of PAN and BAN under  $N_2$  atmosphere obtained at several isothermal temperatures. As it can be seen, both ILs have a significant degradation in short times at temperatures lower than the corresponding  $t_{\text{onset}}$  obtained in dynamic scans. Table 5 shows the mass loss percentage after 50 min at different temperatures, all lower than  $t_{\text{onset}}$ , where it can be seen that EAN and PAN ILs have the same stability, although BAN presents the higher mass loss percentage at 180 °C, as expected for the IL with the lowest  $t_{\text{onset}}$ . This conclusion is also clear in Figure S3 in ESI that shows a comparison of the isothermal behaviour at 180 °C for EAN, PAN and BAN.

Definitely, the onset temperature overestimates the thermal stability, as it has already been pointed out by numerous authors [4, 49–52]. Therefore, for characterizing the long-term stability of these compounds, it is necessary to carry out a more in-depth and exhaustive analysis to establish more realistic parameters as for example the *maximum operation temperature* (MOT) [52]. Considering the small differences between the dynamic stability results obtained in air and  $N_2$  atmospheres, this analysis has only been done under  $N_2$  atmosphere.

**Table 5** Mass loss after 50 min of exposure at the different isothermal temperatures

IL	Temperature/°C	Mass loss/%
EAN	140	3
	160	7
	180	18
PAN	140	2
	160	5
	180	15
BAN	140	2
	160	6
	180	24

**Maximum operation temperature (MOT).** Taking the previous consideration into account, the definition of a parameter that allows the characterization of the thermal stability for different degradation levels was necessary. Up to now, a clear criterion on the maximum degradation level at which the fluid retains its usual properties does not exist. It is possible to find in the literature a wide range of conditions depending on the application and on the mechanism of mass loss [51, 53, 54] as we already emphasized in our study of EAN [15].

In previously reported manuscripts, we introduced and compared different methodologies to calculate the MOT, using dynamic and isothermal scans [10, 15]. In this work we used two different criteria, one based on dynamic study and the other on isothermal study. The first one is the criterion of Wooster et al. [51] that suggested that the indicator of the thermal stability is the temperature at which 1% degradation occurs in 10 h ( $T_{0.01/10\text{ h}}$ ), which is calculated from the equation:

$$T_{0.01/10\text{ h}} = 0.82T_{\left(\frac{dw}{dt}\right) \neq 0} \quad (4)$$

being  $T_{(dw/dt) \neq 0}$  the temperature, in Kelvin, at which the first appreciable mass loss occurs, calculated as the temperature where DTG curve starts to separate from the baseline. Results of the MOT calculated from this method ( $t_{\text{Wooster}}$ ) for the three ILs are presented in Table 6.

The second procedure is proposed by Efimova et al. [52] who took into account an acceptable maximum level of degradation of 1%. They proposed the use of Eq. (5) to calculate the MOT against time of operation ( $t_{\text{max}}$ ):

$$\text{MOT} = \frac{E_A}{R[4.6 + \ln(A \cdot t_{\text{max}})]} \quad (5)$$

where  $E_A$  is the activation energy of degradation process, and A corresponds to the adjusted parameters of Arrhenius equation, which links the rate of loss mass ( $k$ ) of every temperature with  $E_A$  ( $k = A \cdot e^{-\frac{E_A}{RT}}$ ) [7, 10], R the constant of ideal gases and  $t_{\text{max}}$  is the maximum time of exposition.

**Table 6** MOT (in °C) using the criteria of 1% of loss mass in 10 h estimated from Wooster ( $t_{\text{Wooster}}$ ) [51] and Efimova ( $t_{0.01/10\text{ h}}$ ) [52] methods, and adjusted parameters of Arrhenius behaviour for isothermal scans

IL	Temperature Wooster/°C	Activation energy/kJ mol <sup>-1</sup>	lnA	Temperature $t_{0.01/10\text{ h}}$ /°C
EAN	82 ± 5	94 ± 3	24 ± 1	42*
PAN	74 ± 5	86 ± 7	21 ± 2	42*
BAN	78 ± 5	102 ± 8	26 ± 3	55*

\*Uncertainties of this method are estimated in 10–15%

**Fig. 2** Maximum operation temperature (MOT) of the selected ILs

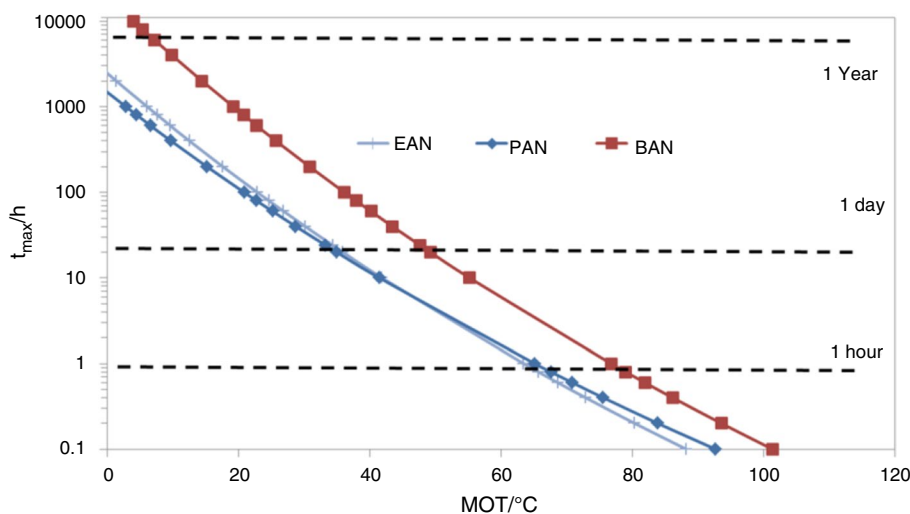


Table 6 presents the values of these adjusted parameters ( $E_A$  and  $\ln A$ ) of Arrhenius equation for these ILs. From these data a chart that relates the MOT and the degradation time is presented in Fig. 2. Additionally, the MOT corresponding to a degradation level of 1% in 10 h was calculated from this chart and expressed in Table 6, obtaining values lower than the corresponding to Wooster methods, similarly that those reported for different ILs and lubricant bases in a previous paper [10].

### Density measurements

Density values for the dried and environmentally saturated ILs in the temperature range from 288 to 368 K are presented in Fig. 3a and summarized in Table S1-ESI.

As it can be seen, density decreases linearly (with similar negative slope) with temperature, as can be expected [22, 55] for all the ILs, dry and water saturated. Fitting parameters are shown in Table 7. The trend followed by this property in dry ILs is  $\rho_{EAN} > \rho_{PAN} > \rho_{BAN}$ , that is the density increases upon the decrease of the alkyl chain length. Despite the different water content of every saturated IL, as we pointed out in Table 2, the water absorbed does not change the trend, although some differences are exposed later in this section.

The trend followed by the density of dry ILs can be explained taking into account the increasing difficulties of forming hydrogen bonds with increasing length of the cation related with increasing electrostatic repulsions, hindering the packing and making less dense the ILs with the longer alkyl chain [26].

Although these ILs are well known, the number of references is scarce. Table S2 ESI shows a comparison between density values for pure ILs and those reported in the literature [26, 44, 48, 56–61]. There is a good agreement in all cases, being the small observed differences associated to

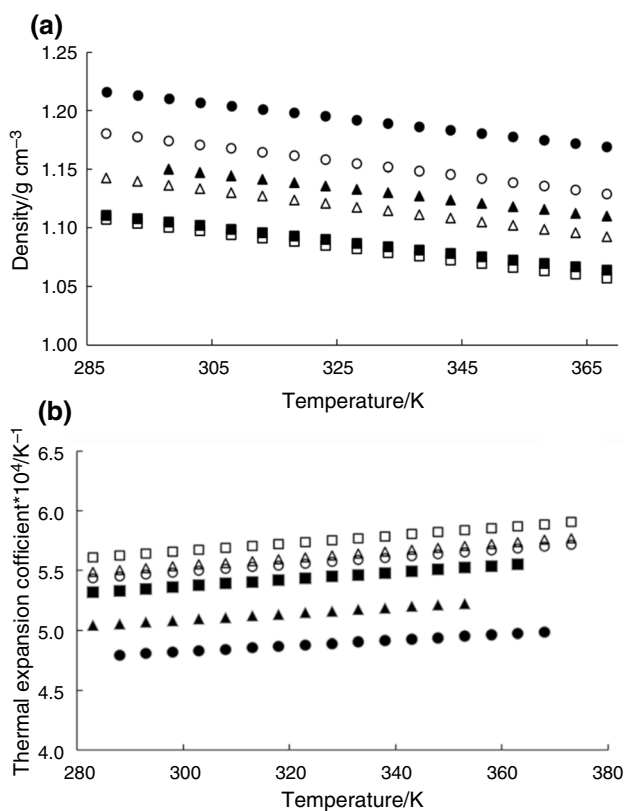


**Fig. 3** (a) Experimental densities and (b) thermal expansion coefficients of the dried and saturated ILs as a function of temperature: (black circle) EAN, (black triangle) PAN and (black square) BAN, (white circle) EAN sat, (white triangle) PAN sat and (white square) BAN sat

possible impurities in the samples or to the different experimental methodology used.

Moreover, it can be observed that the higher the water content, the higher the decrease in density values for the saturated samples regarding pure IL, which is not surprising,



**Table 7** Fitting coefficients obtained from the linear correlation ( $\rho = a + bT$ ) of density and temperature for the dried and saturated ILs

IL		$a \pm s(a)/\text{g cm}^{-3}$	$b \pm s(b)/\text{g cm}^{-3} \text{K}^{-1}/10^{-4}$	$R^2$
EAN	Dried	$1.3839 \pm 0.0005$	$-5.83 \pm 0.02$	0.99998
	Saturated	$1.3663 \pm 0.0002$	$-6.44 \pm 0.01$	0.99998
PAN	Dried	$1.3229 \pm 0.0004$	$-5.79 \pm 0.01$	0.99993
	Saturated	$1.3242 \pm 0.0002$	$-6.29 \pm 0.01$	0.99998
BAN	Dried	$1.2806 \pm 0.0004$	$-5.89 \pm 0.01$	0.99994
	Saturated	$1.2866 \pm 0.0003$	$-6.23 \pm 0.01$	0.99995

due to the lower density of water relative to pure ILs. Thus, for example, at 298 K, density of EAN shows a decrease of 2.97%, 1.20% for PAN and only 0.38% for BAN; all of them calculated relative to the density values of the dried ILs at 298 K. As we pointed out previously, density of water saturated ILs fits well to a linear equation (see Table 7) although the absolute value of the slope is higher than that corresponding to dry ILs.

Also, relatively good agreement with the limited references can be found for the density of water saturated ILs. Thus, Zarrougui et al. [56] determined the dependence of density for the mixture EAN–water at different molar fractions, obtaining for a molar fraction of 0.4210 a density value of  $1169.4 \text{ kg m}^{-3}$  at 298 K, which is next to our value for saturated EAN of  $1174.2 \text{ kg m}^{-3}$  (which corresponds to a EAN mole fraction of 0.426). Segade et al. [58] studied mixtures containing alkyl-ammonium nitrates and water at 298.15 K obtaining for 0.3394 and 0.6031 molar fractions of EAN values of 1163 and  $1191 \text{ kg m}^{-3}$ , respectively, well-matched with our results. These authors also obtained a density value of  $1101.8 \pm 2 \text{ kg m}^{-3}$  for a molar fraction of BAN of 0.638, which is comparable to the value of  $1100.8 \text{ kg m}^{-3}$  here obtained for saturated BAN, whose molar fraction in BAN is 0.565. Xu [61] obtained for this last IL a value of

$1098.8 \pm 0.19 \text{ kg m}^{-3}$ , which is also in good agreement with the results here shown.

From density measurements, the thermal expansion coefficient can be determined. Figure 3b presents the values of this parameter for pure and water saturated ILs, which increases with the chain length of the cation, similarly than Bouzón-Capelo et al. [26] observations. Saturated ILs present higher values of the thermal expansion coefficient than pure ILs, possibly associated to that water solvates the anion-forming clusters and decreasing the coulombic forces in the structure of the ILs [62, 63].

### Heat capacity analysis

The isobaric specific heat capacity ( $c_p$ ), for the dried and saturated ILs between (293.15 and 348.15) K are presented in Fig. 4a and included in Tables S3 and S4 of ESI. Samples were in the liquid state throughout the studied temperature interval. As usual,  $c_p$  increases with temperature. The three ILs here studied have the same anion, and the cation only differs in a methyl group. Nevertheless, light differences in the  $c_p$  values were obtained, being the observed sequence for dried ILs, EAN < PAN < BAN. In case of saturated samples,

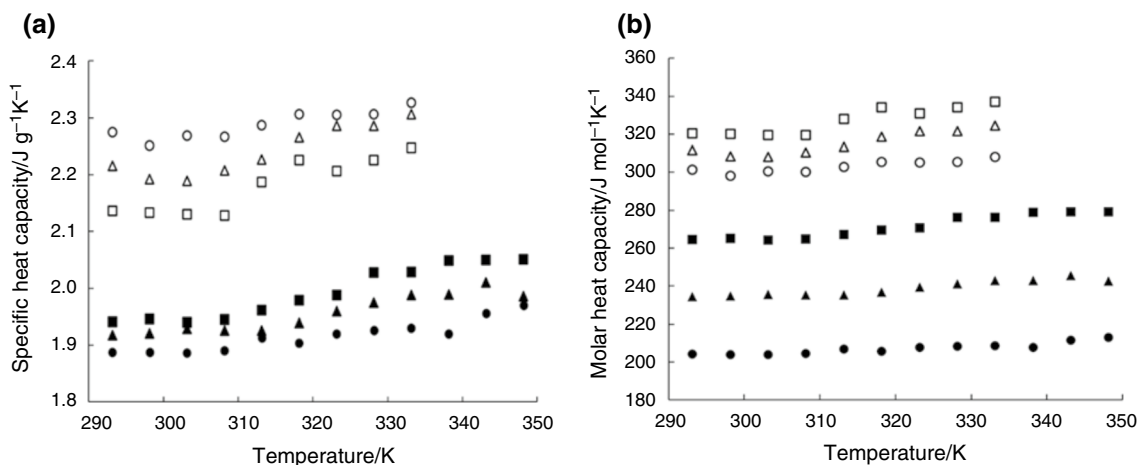


**Fig. 4** Comparisons of isobaric specific (a) and isobaric molar (b) heat capacity for the three, dried and saturated, ILs: (black circle) EAN, (black triangle) PAN, (black square) BAN, (white circle) EAN

sat, (white triangle) PAN sat, and (white square) BAN sat. Experiments were performed at  $(978 \pm 5)$  hPa of atmospheric pressure

the tendency is the opposite,  $EAN > PAN > BAN$ , which is not surprising because the saturated EAN has the higher water content. For example, at 298 K, the per cent change of isobaric specific heat capacity is 19.3% for EAN, 14.1% for PAN and 9.6% for BAN.

The isobaric molar heat capacities values,  $C_p$ , for the selected ILs between (293.15 and 348.15) K are plotted against temperature in Fig. 4b (values are summarized in Tables S3 and S4 of ESI). In this case, the sequence with the temperature for this property is the same for both, dried and water saturated ILs ( $EAN < PAN < BAN$ ). This is in agreement with the observation of Zorebsky et al. [64], which indicates that  $C_p$  often correlates with molar mass, since degrees of freedom of the molecule strongly increase with the alkyl chain length of the cation. This agrees with our experimental data because molar masses are 132.4, 140.7 and 150.0  $\text{g mol}^{-1}$ , for saturated samples of EAN, PAN and BAN, respectively, which means that the tendency in this property does not change with water.

Up to our knowledge, no data about isobaric molar heat capacity can be found in literature for the studied ionic liquids. Only in the case of EAN a value of  $(207.47 \pm 0.51)$   $\text{J mol}^{-1} \text{K}^{-1}$ , obtained through flow calorimetry at 298.15 K, was published by Allen et al. [57], which is in fairly good agreement with the value of  $204.06 \text{ J mol}^{-1} \text{K}^{-1}$  here obtained at the same temperature. The small discrepancy can likely be due to the lower water content in the EAN sample analysed in the present work.

Heat energy storage density, which is directly related to the volumetric heat capacity, is a critical parameter (more important than specific heat) for using these fluids as heat accumulators or heat carriers [65]; thus, higher values of this parameter allow lower temperatures in the bearing gaps [66]. Volumetric heat capacity data corresponding to the

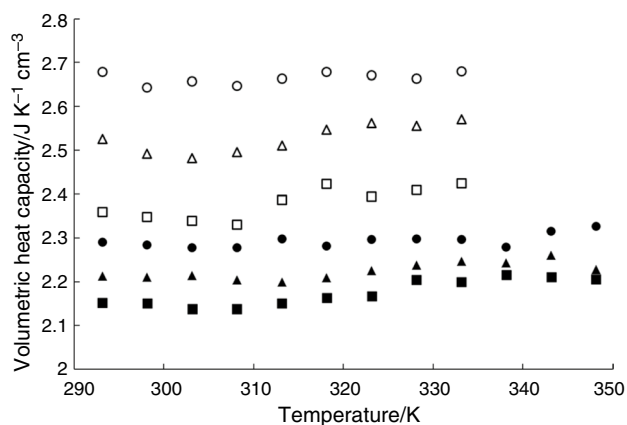


**Fig. 5** Comparison of volumetric heat capacities of the three ILs, dried and saturated respectively: (black circle) EAN, (black triangle) PAN, (black square) BAN, (white circle) EAN sat, (white triangle) PAN sat, and (white square) BAN sat

dried and saturated ILs have been obtained as the product of heat capacity (in  $\text{J g}^{-1} \text{K}^{-1}$ ) and density values (in  $\text{g cm}^{-3}$ ), and they are shown in Fig. 5 and summarized in Tables S3 and S4 (ESI).

Some authors have previously determined volumetric heat capacities of ILs; among them, Salgado et al. [66] have analysed some ILs of the most commonly studied families, imidazolium and pyrrolidinium ones. These authors have observed that the heaviest ILs present higher values of volumetric heat capacities than the light ones, although in the present work this tendency is clearly the opposite  $EAN > PAN > BAN$ , for both pure and saturated ILs. This fact can be explained considering the small differences of the molecular mass of the samples since they just increment in a methyl group among each other. Salgado et al. also found lower values for imidazolium and pyrrolidinium than for those here studied, so the selected compounds of the present manuscript could be better lubricants for hydrodynamic bearings.

### Thermal conductivity analysis

Thermal conductivity of ILs is one of the most important properties of fluids of heat transfer it is one of the least studied, although it is well known that the thermal conductivity for many molecular solvents should decrease with increasing the molecular size of compounds [21].

The thermal conductivity data for the three ILs, both dried and saturated, was studied in the temperature range from (293.15 to 323.15) K. Five values for each temperature and the corresponding mean and standard deviations are presented in Table S5 and Table S6 (see ESI document) for dried and saturated samples, respectively. Figure 6 shows the mean value of the thermal conductivity versus temperature for all the analysed samples. All the liquids exhibited thermal conductivity values within the range (0.19 to 0.25) W

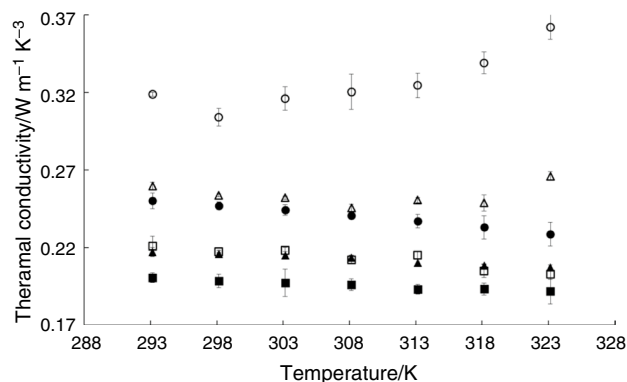


**Fig. 6** Thermal conductivity for the three ILs, dried and saturated: (black circle) EAN, (black triangle) PAN, (black square) BAN, (white circle) EAN sat, (white triangle) PAN sat and (white square) BAN sat

$\text{m}^{-1} \text{K}^{-1}$ , according to previously reported data [24]. These PILs show higher values of this property than other ILs, as can be seen in the literature [21, 67], similar and even higher than other conventional solvents as ethylene glycol, methanol and toluene, although these values are always lower than the corresponding to water. [67].

Cation alkyl chain length has an important effect on this property, decreasing with the number of alkyl groups, similarly to density [26], and PILs seems to have higher values of thermal conductivity than APILs, due to the extensive H-bonding structure [24]. Thermal conductivity behaviour can be explained by the pseudolattice phonon hopping model, widely described by Carrete et al. [25] and Murphy et al. [24]. These authors point out that thermal conduction can be associated to the vibrations generated in the polar regions of the ILs, which is similar for the three ILs here studied, whereas the apolar domains, the alkyl chain, presents a barrier to phonon hopping, which increases with its length, provoking a decrease in this property.

In the case of dried samples of the three ILs, a linear dependence between the temperature and the thermal conductivity was found. A slightly decrease of the thermal conductivities of each IL was observed as the temperature increases, as it was pointed out by other authors for similar and other ILs [24, 68, 69]. The experimental data for dried samples were fitted with a linear correlation with temperature. Table 8 collects the parameters of the linear fitting for each IL. This type of simple correlation is very useful for engineering applications involving heat transfer over a range of temperatures.

A significant increase on the thermal conductivity with water content was observed, being all saturated ILs thermal conductivity values within the range (0.20 to 0.37)  $\text{W} \cdot \text{m}^{-1} \text{K}^{-1}$ , as can be also seen in Fig. 6. Up to our knowledge, no data have been reported in the literature for the thermal conductivity of mixtures of these ILs and water, except for PAN-water mixtures at the unique temperature of 293 K in the study of Murphy et al. [24]. In that work, for a molar fraction of PAN of 0.45, a value of 0.25  $\text{W} \cdot \text{m}^{-1} \text{K}^{-1}$  can be estimated from the manuscript figure, which is in good agreement with the value of 0.2598  $\text{W} \cdot \text{m}^{-1} \text{K}^{-1}$  here reported for PAN saturated sample with molar fraction of 0.493. These researchers attribute this increase to changes

in the nanostructure of the phonon hopping pseudolattice in the sense of the water swells the polar domain reducing the relation apolar/polar volume fraction, and hence decreasing the barrier to phonon hopping.

As can be seen in Fig. 6 the water content seems to have an important effect on the behaviour of this property with temperature of saturated ILs. Thus, while the thermal conductivity of dry EAN decreases with temperature, this tendency changes for the saturated sample from 298 K and the thermal conductivity increases with temperature. This phenomenon may be due to the fact that this IL showed the highest water content, and the thermal conductivity of water increases with increasing temperature [70]. A similar effect, but less intense, was observed for saturated PAN, whose minimum is observed at higher temperatures than EAN. In case of saturated BAN, whose water content was the lowest, no significant changes in the decreasing tendency were observed when comparing with the dried sample. In terms of the so-called enhancement of the thermal conductivity [21], that is the change of the thermal conductivity relative to the value for the dried IL, the larger change was observed for EAN, that oscillated between 27% at 293 K to 58% at 323 K, followed by PAN with values between 20 and 28% for the same temperatures, and finally by BAN whose values were almost independent of temperature, varying between 10 and 6%, at 293 and 323 K respectively.

## Rheological measurements

Dynamic viscosities of dried and saturated samples were determined using a viscometer Anton Paar Stabinger SVM3000 and a TA Instruments AR2000 stress control rheometer, following the methodology indicated in materials and methods section. A preliminary study was performed by means of continuous flow experiments using the Peltier device and the cone geometry previously mentioned to determine the linear viscoelastic region (LVR) of the six selected fluids. In all cases a broad interval was obtained; the three ILs showed a Newtonian behaviour from 1 to  $10^5 \text{ s}^{-1}$  of shear rate. A proper knowledge of this region allows the correct selection of the parameters employed in the following oscillatory temperature sweep experiments, whose procedure was detailed in the section of Materials and methods. In Tables S7 and S8 (in ESI) viscosity values for dried and saturated samples obtained using Anton Paar Stabinger viscometer and TA AR2000 rheometer, respectively, are shown. Figure 7 shows the obtained values for dynamic viscosity using these two techniques for the dried and saturated samples. Small differences have been detected between viscosity values obtained by means of the two techniques. This disparity can be due to the difference between experimental procedures to obtain the values of the viscosity. In case of the

**Table 8** Fitting parameters (*a* and *b*) for linear equation between thermal conductivity (*k*) and temperature (*T*, in Kelvin) ( $k = a + bT$ ) corresponding to dried samples

	$a \pm s(a)/\text{W} \cdot \text{m}^{-1} \text{K}^{-1}$	$10^4$ $b \pm s(b)/\text{W} \cdot \text{m}^{-1} \text{K}^{-2}$
EAN	$0.460 \pm 0.008$	$-7.1 \pm 0.3$
PAN	$0.320 \pm 0.009$	$-3.5 \pm 0.3$
BAN	$0.284 \pm 0.008$	$-2.9 \pm 0.3$

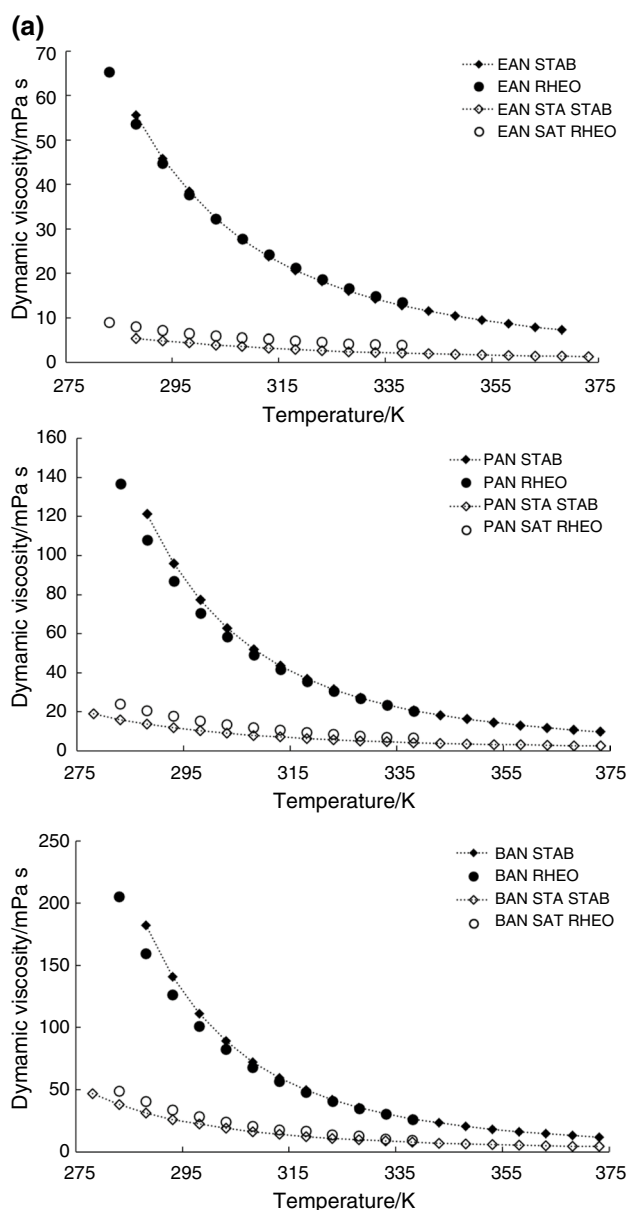


**Fig. 7** Dynamic viscosity obtained from rheological (RHEO) and viscometer (STAB) experiments for the dried and saturated ILs. Lines were introduced to better visualize the tendency

viscometer, the sample is all time in a closed tube, but not in the case of the rheometer, where the side edge of the sample is surrounded by air. To avoid as much as possible the interaction of the sample with the surrounding air, a lid was put around the geometry and the sample. As it can be seen in Fig. 7, the largest discrepancies have been obtained for saturated samples. This is probably due to the huge instability of the water content on the saturated samples, which, as it was cited before, can easily change with small alterations on the environmental humidity. In case of dried

samples, these differences are much lower and decrease as the temperature increases.

As it can also be observed in Fig. 7, for all studied samples, viscosity decreases with increasing temperature. As the viscosity decreases with temperature, the effect of water is much less important, as it was previously pointed out by Jacquemin *et al.* [71].

In Fig. 8a comparison of viscosity of dried ILs (a) and saturated ILs (b), using the Anton Paar viscometer, is shown. Viscosity increases with increasing alkyl chain length, as some authors have previously reported [62, 71, 72].

An important reduction of the viscosity with the absorption of water can be observed for the three ILs, ranging from more than 90% for EAN, 89% for PAN and 83% for BAN at lowest studied temperatures. The trend with alkyl chain length is the same than that observed from dried ILs. This change in viscosity, which also appears in other transport properties such as electrical conductivity [27], can be especially important for designing humidity sensors.

Table S9 ESI collects a comparison of the viscosity data here shown with those presented in the literature for dried samples [44, 48, 56, 59, 61, 73, 74]. In almost all cases, experimental values are comparable with that reported by the other authors.

In the case of saturated samples, less data have been reported. Zarrougui *et al.* [56] presented a viscosity value of  $(5.03 \pm 0.12)$  mPa s at 293.15 K for a mixture EAN + water in a molar fraction of EAN 0.421 that is near the value of 4.86 mPa s here obtained at the same temperature for saturated EAN with 0.426 molar fraction. Xu [61] reported values of  $(26.25 \pm 0.57)$  and  $(15.1 \pm 0.33)$  mPa s for a mixture BAN + water with molar fractions in the IL of 0.6505 and 0.5011, respectively, at 298.15 K, that are in concordance with the value of 22.32 mPa s here obtained for saturated BAN (with an IL molar fraction of 0.565) at the same temperature.

Many studies reviewed that ILs, protic and aprotic, do not follow Arrhenius behaviour, due to the well-known glass-forming tendency of these liquids, even in mixtures with water [75]. The Vogel–Fulcher–Tamman (VFT) equation (Eq. 6) is one the most used for bringing in the temperature dependence of the viscosity:

$$\eta = \eta_0 \exp\left(\frac{E_a/R}{T - T_g}\right) \quad (6)$$

Being  $\eta_0$ ,  $T_g$  and  $E_a$  adjustable VFT parameters;  $T_g$  is a temperature 50 K lower than glass transition temperature of the material.

In Table 9, parameters obtained from the fittings of viscosity experimental results to VFT equations are shown.

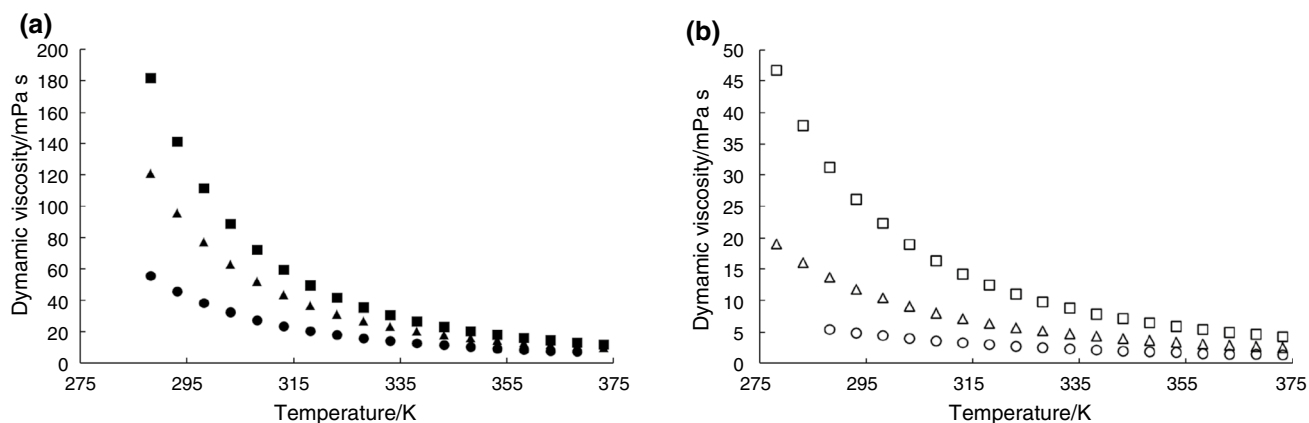


**Fig. 8** Comparison of dynamic viscosities obtained from viscosimeter experiments for dried **(a)** and saturated **(b)** ILs: EAN (circle symbol), PAN (triangle symbol) and BAN (square symbol)

**Table 9** Fitting parameters of experimental viscosity data (RHEO: rheometer, STAB: Stabinger) of the studied ILs to Vogel–Fulcher–Tamman equation and those reported in Canongia et al. [44] for dried samples

		$\eta_0 \pm s(\eta_0)/\text{mPa s}$	$E_a \pm s(E_a)/\text{J mol}^{-1}$	$T_g \pm s(T_g)/\text{K}$	$R^2$
EAN	RHEO	$0.29 \pm 0.02$	$6050 \pm 140$	$149 \pm 2$	0.999998
	STAB	$0.206 \pm 0.009$	$6160 \pm 120$	$148 \pm 1$	0.999997
	Canongia et al.	0.2199	6362	148.5	
EAN SAT	RHEO	$0.2 \pm 0.1$	$6000 \pm 2000$	$120 \pm 40$	0.9997
	STAB	$0.06 \pm 0.02$	$7200 \pm 1000$	$100 \pm 15$	0.9997
PAN	REO	$0.25 \pm 0.02$	$6740 \pm 150$	$154 \pm 2$	0.999997
	STAB	$0.193 \pm 0.006$	$7090 \pm 80$	$156 \pm 1$	0.999997
	Canongia et al.	0.2082	6950	156.1	
PAN SAT	RHEO	$0.19 \pm 0.03$	$6000 \pm 400$	$136 \pm 5$	0.99998
	STAB	$0.110 \pm 0.007$	$6350 \pm 190$	$130 \pm 3$	0.99998
BAN	RHEO	$0.159 \pm 0.009$	$8180 \pm 150$	$146 \pm 18$	0.999998
	STAB	$0.159 \pm 0.005$	$7790 \pm 80$	$155 \pm 1$	0.999998
	Canongia et al.	0.2203	6956	162.9	
BAN SAT	RHEO	$0.14 \pm 0.11$	$7000 \pm 2000$	$140 \pm 20$	0.9996
	STAB	$0.15 \pm 0.01$	$6500 \pm 200$	$143 \pm 3$	0.999998

As it can be seen in Table 9, although in all cases  $R^2 \cong 0.99$ , the lowest uncertainties were obtained for dried samples, regardless of the experimental procedure. The obtained VFT parameters are in good agreement with those obtained by other authors for similar ILs, as it is shown in this table.

## Conclusions

A thermophysical characterization of three ILs with ammonium cations of different alkyl chain length and nitrate common anion was performed in this work. The main conclusions are the following:

- The three ILs showed a crystalline behaviour, characterized by a freezing process (exothermic peak in

cooling ramp) and a melting process (endothermic peak in heating ramp). A clear supercooling effect can be observed for the three ILs. The melting temperature follows the trend: PAN < EAN < BAN.

- These ILs present similar onset temperatures in TG experiences, between 230 and 245 °C, which are lower than the corresponding to aprotic ILs, although the alkyl chain length tends to slightly reduce the thermal stability. The main mechanism involved in the mass loss process seems to be evaporation.
- Density of pure ILs is higher than density of saturated ILs throughout the entire temperature interval. This property decreases with the temperature as can be expected and the rate of decrease (slope of the fit) is similar for pure and saturated ILs. Density also decreases with increasing the alkyl chain length for both, dry and water saturated ILs.

- The trend for isobaric specific heat for pure ILs is  $EAN < PAN < BAN$ , although the tendency is the opposite for saturated ILs,  $EAN > PAN > BAN$ , reflecting the trend of water saturated content for these ILs.
- The sequence followed by the thermal conductivity obtained for dried ILs,  $EAN > PAN > BAN$  agrees with the fact that the cation alkyl chain length has an important effect on this property. In case of dried samples of the three ILs, a linear dependence between the temperature and the thermal conductivity was found, decreasing slightly with temperature. For saturated samples, the sequence mentioned above was inverted, due to the strong effect of water on this property. Thus, at 293 K, an enhancement of 27% was obtained for EAN, whereas for PAN and BAN were 20% and 10% respectively.
- Similar values of dynamic viscosity of dried and saturated ILs are obtained using two different techniques, rheometry and viscometry. In all cases, this property decreases with temperature and with water uptake, as expected, and experimental values follow with high correlation the VFT equation. Dried and water saturated ILs presented the same tendency with the alkyl chain length  $BAN > PAN > EAN$ .

Results here presented can strengthen the applicability of these protic ammonium ILs, for example, as low temperature HTFs fluids or absorbents of heat pumps, especially taking into account the transport properties improvement, for this application, with the absorption of water.

**Supplementary Information** The online version contains supplementary material available at <https://doi.org/10.1007/s10973-023-12194-1>.

**Acknowledgements** Authors acknowledge M. Gómez (RIAIDT-USC) for the technical support in DSC and TGA measurements. This work was supported by Spanish Ministry of Economy and Competitiveness and FEDER Program through the projects MAT2017-89239-C2-1-P, PID2020-112846RB-C22 as well as by Xunta de Galicia through GRC ED431C 2020/10 project and the Galician Network of Ionic Liquids (ReGaLIs) ED431D 2017/06. P. Vallet thanks funding support of FPI Program from Spanish Ministry of Science and J. J. Parajó and M. J. G. Guimarey thank the I2C postdoctoral Program of the Xunta de Galicia, for their support in funding the study.

**Funding** Open Access funding provided thanks to the CRUE-CSIC agreement with Springer Nature.

**Open Access** This article is licensed under a Creative Commons Attribution 4.0 International License, which permits use, sharing, adaptation, distribution and reproduction in any medium or format, as long as you give appropriate credit to the original author(s) and the source, provide a link to the Creative Commons licence, and indicate if changes were made. The images or other third party material in this article are included in the article's Creative Commons licence, unless indicated otherwise in a credit line to the material. If material is not included in the article's Creative Commons licence and your intended use is not permitted by statutory regulation or exceeds the permitted use, you will need to obtain permission directly from the copyright holder. To view a copy of this licence, visit <http://creativecommons.org/licenses/by/4.0/>.

## References

1. Emel'Yanenko VN, Boeck G, Verevkin SP, Ludwig R. Volatile times for the very first ionic liquid: understanding the vapor pressures and enthalpies of vaporization of ethylammonium nitrate. *Chem A Eur J*. 2014;20:11640–5. <https://doi.org/10.1002/chem.201403508>.
2. Lee SY, Yasuda T, Watanabe M. Fabrication of protic ionic liquid/sulfonated polyimide composite membranes for non-humidified fuel cells. *J Power Sour*. 2010;195:5909–14. <https://doi.org/10.1016/j.jpowsour.2009.11.045>.
3. Reiter J, Paillard E, Grande L, Winter M, Passerini S. Physicochemical properties of N-methoxyethyl-N-methylpyrrolidinium ionic liquids with perfluorinated anions. *Electrochim Acta*. 2013;91:101–7. <https://doi.org/10.1016/j.electacta.2012.12.086>.
4. Parajó JJ, Teijeira T, Fernández J, Salgado J, Villanueva M. Thermal stability of some imidazolium [NTf<sub>2</sub>] ionic liquids: Isothermal and dynamic kinetic study through thermogravimetric procedures. *J Chem Thermodyn*. 2017. <https://doi.org/10.1016/j.jct.2017.04.016>.
5. Parajó JJ, Villanueva M, Troncoso J, Salgado J. Thermophysical properties of choline and pyridinium based ionic liquids as advanced materials for energy applications. *J Chem Thermodyn*. 2020;141:105947. <https://doi.org/10.1016/j.jct.2019.105947>.
6. Parajó JJ, Vallet P, Varela LM, Villanueva M, Salgado J. Ecotoxicity of binary mixtures of ILs and inorganic salts of electrochemical interest. *Environ Sci Pollut Res*. 2021. <https://doi.org/10.1007/s11356-021-17515-1>.
7. Parajó JJ, Villanueva M, Salgado J. Thermal stability of ionic liquids, In: Seijas J, Vázquez P editors, *Ion. Liq. Synth. Prop. Technol. Appl.*, MDPI, Berlin, 2019. pp. 1–16. <https://doi.org/10.1515/9783110583632>.
8. Sánchez PB, García J, Salgado J, González-Romero E. Studies of volumetric and transport properties of ionic liquid-water mixtures and its viability to be used in absorption systems. *ACS Sustain Chem Eng*. 2016. <https://doi.org/10.1021/acssuschemeng.6b01541>.
9. Salgado J, Teijeira T, Parajó JJ, Fernández J, Troncoso J. Isobaric heat capacity of nanostructured liquids with potential use as lubricants. *J Chem Thermodyn*. 2018. <https://doi.org/10.1016/j.jct.2018.03.031>.
10. Parajó JJ, Villanueva M, Otero I, Fernández J, Salgado J. Thermal stability of aprotic ionic liquids as potential lubricants. Comparison with synthetic oil bases. *J Chem Thermodyn*. 2018;116:185–96. <https://doi.org/10.1016/j.jct.2017.09.010>.
11. Xue Z, Qin L, Jiang J, Mu T, Gao G. Thermal, electrochemical and radiolytic stabilities of ionic liquids. *Phys Chem Chem Phys*. 2018;20:8382–402. <https://doi.org/10.1039/c7cp07483b>.
12. Cera-Manjarres A, Salavera D, Coronas A. Vapour pressure measurements of ammonia/ionic liquids mixtures as suitable alternative working fluids for absorption refrigeration technology. *Fluid Phase Equilib*. 2018;476:48–60. <https://doi.org/10.1016/j.fluid.2018.01.006>.
13. Xie H, Zhao Z, Zhao J, Gao H. Measurement of thermal conductivity, viscosity and density of ionic liquid [EMIM][DEP]-based nanofluids, Chinese. *J Chem Eng*. 2016;24:331–8. <https://doi.org/10.1016/j.cjche.2015.11.024>.
14. Yasuda T, Kinoshita H, Miran MS, Tsuzuki S, Watanabe M. Comparative study on physicochemical properties of protic ionic liquids based on allylammonium and propylammonium cations. *J Chem Eng Data*. 2013;58:2724–32. <https://doi.org/10.1021/je301284x>.
15. Salgado J, Parajó JJ, Villanueva M, Rodríguez JR, Cabeza O, Varela LM. Liquid range of ionic liquid – Metal salt

- mixtures for electrochemical applications. *J Chem Thermodyn*. 2019;134:164–74. <https://doi.org/10.1016/j.jct.2019.03.012>.
16. Vallet P, Bouzón-Capelo S, Méndez-Morales T, Gómez-González V, Arosa Y, de la Fuente R, López-Lago E, Rodríguez JR, Gallego LJ, Parajó JJ, Salgado J, Turmine M, Segade L, Cabeza O, Varela LM. On the physical properties of mixtures of nitrate salts and protic ionic liquids. *J Mol Liq*. 2022;350:118483. <https://doi.org/10.1016/j.molliq.2022.118483>.
  17. Cabeza O, Varela LM, Rilo E, Segade L, Domínguez-Pérez M, Ausín D, de Pedro I, Fernández JR, González J, Vázquez-Tato MP, Arosa Y, López-Lago E, de la Fuente R, Parajó JJ, Salgado J, Villanueva M, Matveev V, Ievlev A, Seijas JA. Synthesis, microstructure and volumetry of novel metal thiocyanate ionic liquids with [BMIM] cation. *J Mol Liq*. 2019;283:638–51. <https://doi.org/10.1016/j.molliq.2019.03.088>.
  18. Smiglak M, Pringle JM, Lu X, Han L, Zhang S, Gao H, MacFarlane DR, Rogers RD. Ionic liquids for energy, materials, and medicine. *Chem Commun*. 2014;50:9228–50. <https://doi.org/10.1039/c4cc02021a>.
  19. Van Valkenburg ME, Vaughn RL, Williams M, Wilkes JS. Thermochemistry of ionic liquid heat-transfer fluids. *Thermochim Acta*. 2005;425:181–8. <https://doi.org/10.1016/j.tca.2004.11.013>.
  20. Holbrey JD. Heat capacities of common ionic liquids - Potential applications as thermal fluids. *Chim OGGI-Chem Today*. 2007;25:24–6.
  21. Oster K, Goodrich P, Jacquemin J, Hardacre C, Ribeiro APC, Elsinawi A. A new insight into pure and water-saturated quaternary phosphonium-based carboxylate ionic liquids: Density, heat capacity, ionic conductivity, thermogravimetric analysis, thermal conductivity and viscosity. *J Chem Thermodyn*. 2018;121:97–111. <https://doi.org/10.1016/j.jct.2018.02.013>.
  22. Salgado J, Regueira T, Lugo L, Vijande J, Fernández J, García J. Density and viscosity of three (2,2,2-trifluoroethanol+1-butyl-3-methylimidazolium) ionic liquid binary systems. *J Chem Thermodyn*. 2014;70:101–10. <https://doi.org/10.1016/j.jct.2013.10.027>.
  23. He Z, Zhao Z, Zhang X, Feng H. Thermodynamic properties of new heat pump working pairs: 1,3-Dimethylimidazolium dimethylphosphate and water, ethanol and methanol. *Fluid Phase Equilib*. 2010;298:83–91. <https://doi.org/10.1016/j.fluid.2010.07.005>.
  24. Murphy T, Varela LM, Webber GB, Warr GG, Atkin R. Nanostructure-thermal conductivity relationships in protic ionic liquids. *J Phys Chem B*. 2014;118:12017–24. <https://doi.org/10.1021/jp507408r>.
  25. Carrete J, Méndez-Morales T, García M, Vila J, Cabeza Ó, Gallego LJ, Varela LM. Thermal conductivity of Ionic Liquids: a pseudolattice approach. *J Phys Chem C*. 2012;116:1265–73. <https://doi.org/10.1021/jp208972t>.
  26. Bouzón-Capelo S, Méndez-Morales T, Carrete J, López Lago E, Vila J, Cabeza O, Rodríguez JR, Turmine M, Varela LM. Effect of temperature and cationic chain length on the physical properties of ammonium nitrate-based protic ionic liquids. *J Phys Chem B*. 2012;116:11302–12. <https://doi.org/10.1021/jp3066822>.
  27. Ausín D, Parajó JJ, Trenzado JL, Varela LM, Cabeza O, Segade L. Influence of small quantities of water on the physical properties of alkylammonium nitrate ionic liquids. *Int J Mol Sci*. 2021. <https://doi.org/10.3390/ijms22147334>.
  28. Parajó JJ, Villanueva M, Sánchez PB, Salgado J. Liquid window of some biologically-active ionic liquids. *J Chem Thermodyn*. 2018;126:1–10. <https://doi.org/10.1016/j.jct.2018.06.014>.
  29. Lorenzo M, Vilas M, Verdía P, Villanueva M, Salgado J, Tojo E. Long-term thermal stabilities of ammonium ionic liquids designed as potential absorbents of ammonia. *RSC Adv*. 2015. <https://doi.org/10.1039/c5ra03192c>.
  30. Salgado J, Villanueva M, Núñez-Fernández O, Proupín-Castiñeiras J, Barros N, Rodríguez-Añón JA. Calorimetric seasonal characterization of culture and pasture soils. *J Therm Anal Calorim*. 2009. <https://doi.org/10.1007/s10973-009-0296-9>.
  31. Gaciño FM, Regueira T, Lugo L, Comuñas MJP, Fernández J. Influence of molecular structure on densities and viscosities of several Ionic Liquids. *J Chem Eng Data*. 2011;56:4984–99. <https://doi.org/10.1021/je200883w>.
  32. Lugo L, Segovia JJ, Martín MC, Fernández J, Villamañán MA. An experimental setup for isobaric heat capacities for viscous fluids at high pressure: squalane, bis(2-ethylhexyl) sebacate and bis(2-ethylhexyl) phthalate. *J Chem Thermodyn*. 2012;49:75–80. <https://doi.org/10.1016/j.jct.2012.01.011>.
  33. Coelho de Sousa Marques MA, Guimarey MJG, Domínguez-Arca V, Amigo A, Fernández J. Heat capacity, density, surface tension, and contact angle for polyalphaolefins and ester lubricants. *Thermochim Acta*. 2021. <https://doi.org/10.1016/j.tca.2021.178994>.
  34. Cerdeiriña CA, Míguez JA, Carballo E, Tovar CA, de la Puente E, Romaní L. Highly precise determination of the heat capacity of liquids by DSC: calibration and measurement. *Thermochim Acta*. 2000;347:37–44. [https://doi.org/10.1016/S0040-6031\(99\)00414-1](https://doi.org/10.1016/S0040-6031(99)00414-1).
  35. Healy J, De Groot J, Kestin J. The theory of the transient hot-wire method for measuring thermal conductivity. *Phys B+C*. 1976;82:392–408. [https://doi.org/10.1016/0378-4363\(76\)90203-5](https://doi.org/10.1016/0378-4363(76)90203-5).
  36. Tomida D. Thermal Conductivity of Ionic Liquids, In: Shahzad A editor, *Impact of Thermal Conductivity on Energy Technologies*, IntechOpen, London, 2018. pp. 17–31. <https://doi.org/10.5772/intechopen.76559>.
  37. López-Sánchez F, Otero I, López ER, Fernández J. Tribological behavior of two 1-ethyl-3-methylimidazolium alkyl sulfates as neat lubricants for a steel-steel contact. *Tribol Trans* In press. 2017. <https://doi.org/10.1080/10402004.2016.1207829>.
  38. Otero I, López ER, Reichelt M, Villanueva M, Salgado J, Fernández J. Ionic liquids based on phosphonium cations As neat lubricants or lubricant additives for a steel/steel contact. *ACS Appl Mater Interfaces*. 2014;6:13115–28. <https://doi.org/10.1021/am502980m>.
  39. Anareddy RS, Lucio AJ, Shaw SK. Adventitious water sorption in a hydrophilic and a hydrophobic ionic liquid: analysis and implications. *ACS Omega*. 2016;1:407–16. <https://doi.org/10.1021/acsomega.6b00104>.
  40. Villanueva M, Fernández-Leira C, Parajó JJ, Fernández-Míguez L, Salgado J. Thermal stability of ionic liquids, In: Seijas J, Vázquez P editors, *Proceedings, MDPI, Berlin, 2019*. P. 58. <https://doi.org/10.3390/ecsoc-22-05791>.
  41. Gómez E, Calvar N, Domínguez Á. Thermal behaviour of pure Ionic Liquids, In: Handy S, editor. *Ionic Liquids Current State of the Art*, INTECH, 2012. pp. 135–152. <https://doi.org/10.5772/67458>.
  42. Atkin R, Warr GG. The smallest amphiphiles: Nanostructure in protic room-temperature ionic liquids with short alkyl groups. *J Phys Chem B*. 2008;112:4164–6. <https://doi.org/10.1021/jp801190u>.
  43. Vázquez-Fernández I. Ph-D Thesis: studies of hydrogen bonding in protonic ionic liquids and their binary mixtures., The Queen's University of Belfast, 2018
  44. Canongia Lopes JN, Esperança JMSS, De Ferro AM, Pereira AB, Plechkova NV, Rebelo LPN, Seddon KR, Vázquez-Fernández I. Protonic ammonium nitrate ionic liquids and their mixtures: insights into their thermophysical behavior. *J Phys Chem B*. 2016;120:2397–406. <https://doi.org/10.1021/acs.jpcc.5b11900>.
  45. Salgado J, Villanueva M, Parajó JJ, Fernández J. Long-term thermal stability of five imidazolium ionic liquids. *J Chem*

- Thermodyn. 2013;65:184–90. <https://doi.org/10.1016/j.jct.2013.05.049>.
46. Parajó JJ, Teijeira T, Fernández J, Salgado J, Villanueva M. Thermal stability of some imidazolium [NTf<sub>2</sub>] ionic liquids: isothermal and dynamic kinetic study through thermogravimetric procedures. *J Chem Thermodyn.* 2017;112:105–13. <https://doi.org/10.1016/j.jct.2017.04.016>.
  47. Cao Y, Mu T. Comprehensive investigation on the thermal stability of 66 ionic liquids by thermogravimetric analysis. *Ind Eng Chem Res.* 2014;53:8651–64.
  48. Greaves TL, Weerawardena A, Fong C, Krodkiewska I, Drummond CJ. Protic ionic liquids: solvents with tunable phase behavior and physicochemical properties. *J Phys Chem B.* 2006;110:22479–87. <https://doi.org/10.1021/jp0634048>.
  49. Blanco D, Bartolomé M, Ramajo B, Viesca JL, González R, Hernández BA. Isoconversional kinetic analysis applied to five phosphonium cation-based ionic liquids. *Thermochim Acta.* 2017;648:62–74. <https://doi.org/10.1016/j.tca.2016.12.014>.
  50. Rajeshwari P. Kinetic analysis of the non-isothermal degradation of high-density polyethylene filled with multi-wall carbon nanotubes. *J Therm Anal Calorim.* 2016;123:1523–44. <https://doi.org/10.1007/s10973-015-5021-2>.
  51. Wooster TJ, Johanson KM, Fraser KJ, MacFarlane DR, Scott JL. Thermal degradation of cyano containing ionic liquids. *Green Chem.* 2006;8:691–6. <https://doi.org/10.1039/b606395k>.
  52. Efimova A, Pfützer L, Schmidt P. Thermal stability and decomposition mechanism of 1-ethyl-3-methylimidazolium halides. *Thermochim Acta.* 2015;604:129–36. <https://doi.org/10.1016/j.tca.2015.02.001>.
  53. Seeberger A, Andresen A-K, Jess A. Prediction of long-term stability of ionic liquids at elevated temperatures by means of non-isothermal thermogravimetric analysis. *Phys Chem Chem Phys.* 2009;11:9375–81. <https://doi.org/10.1039/b909624h>.
  54. Liang R, Yang M, Xuan X. Thermal stability and thermal decomposition kinetics of 1-butyl-3-methylimidazolium dicyanamide, Chinese. *J Chem Eng.* 2010;18:736–41. [https://doi.org/10.1016/S1004-9541\(09\)60122-1](https://doi.org/10.1016/S1004-9541(09)60122-1).
  55. Sánchez PB, Currás MR, Mato MM, Salgado J, García J. Density and viscosity study of pyridinium based ionic liquids as potential absorbents for natural refrigerants: Experimental and modelling. *Fluid Phase Equilib.* 2015;405:37–45. <https://doi.org/10.1016/j.fluid.2015.06.043>.
  56. Zarrougui R, Dhahbi M, Lemordant D. Transport and thermodynamic properties of ethylammonium nitrate – water binary mixtures: effect of temperature and composition. *J Solut Chem.* 2015;44:686–702. <https://doi.org/10.1007/s10953-014-0283-z>.
  57. Allen M, Evans DF, Lumry R. Thermodynamic properties of the ethylammonium nitrate + water system: partial molar volumes, heat capacities, and expansivities. *J Solution Chem.* 1985;14:549–60.
  58. Segade L, Cabanas M, Domínguez-Pérez M, Rilo E, García-Garabal S, Turmine M, Varela LM, Gómez-González V, Docampo-Alvarez B, Cabeza O. Surface and bulk characterisation of mixtures containing alkylammonium nitrates and water or ethanol: experimental and simulated properties at 298.15 K. *J Mol Liq.* 2016;222:663–70. <https://doi.org/10.1016/j.molliq.2016.07.107>.
  59. Nazet A, Weiß L, Buchner R. Dielectric relaxation of nitromethane and its mixtures with ethylammonium nitrate: Evidence for strong ion association induced by hydrogen bonding. *J Mol Liq.* 2017;228:81–90. <https://doi.org/10.1016/j.molliq.2016.09.008>.
  60. Russina O, Mariani A, Caminiti R, Triolo A. Structure of a binary mixture of ethylammonium nitrate and methanol. *J Solution Chem.* 2015;44:669–85. <https://doi.org/10.1007/s10953-015-0311-7>.
  61. Xu Y. Volumetric, viscosity, and electrical conductivity properties of aqueous solutions of two n-butylammonium-based protic ionic liquids at several temperatures. *J Chem Thermodyn.* 2013;64:126–33. <https://doi.org/10.1016/j.jct.2013.05.019>.
  62. Seddon KR, Stark A, Torres MJ. Influence of chloride, water, and organic solvents on the physical properties of ionic liquids. *Pure Appl Chem.* 2000;72:2275–87. <https://doi.org/10.1351/pac200072122275>.
  63. Carvalho PJ, Regueira T, Santos LMNBF, Fernandez J, Coutinho JAP. Effect of water on the viscosities and densities of 1-butyl-3-methylimidazolium dicyanamide and 1-butyl-3-methylimidazolium tricyanomethane at atmospheric pressure. *J Chem Eng Data.* 2010;55:645–52. <https://doi.org/10.1021/je900632q>.
  64. Zorębski E, Zorębski M, Dzida M, Goodrich P, Jacquemin J. Isobaric and isochoric heat capacities of imidazolium-based and pyrrolidinium-based ionic liquids as a function of temperature: modeling of isobaric heat capacity. *Ind Eng Chem Res.* 2017;56:2592–606. <https://doi.org/10.1021/acs.iecr.6b04780>.
  65. Paulechka YU, Kabo AG, Blokhin AV, Kabo GJ, Shevelyova MP. Heat capacity of ionic liquids: Experimental determination and correlations with molar volume. *J Chem Eng Data.* 2010;55:2719–24. <https://doi.org/10.1021/je900974u>.
  66. Salgado J, Teijeira T, Parajó JJ, Fernández J, Troncoso J. Isobaric heat capacity of nanostructured liquids with potential use as lubricants. *J Chem Thermodyn.* 2018;123:107–16. <https://doi.org/10.1016/j.jct.2018.03.031>.
  67. Ge R, Hardacre C, Nancarrow P, Rooney DW. Thermal conductivities of ionic liquids over the temperature range from 293 K to 353 K. *J Chem Eng Data.* 2007;52:1819–23. <https://doi.org/10.1021/je700176d>.
  68. Franca JMP, Lourenco MJV, Sohel Murshed M, Padua AAH, Nieto de Castro CA. Thermal conductivity of ionic liquids and ionanofluids and their feasibility as heat transfer fluids. *Ind Eng Chem Res.* 2018;57:6516–29. <https://doi.org/10.1021/acs.iecr.7b04770>.
  69. Shojaee SA, Farzam S, Hezave AZ, Lashkarbolooki M, Ayatollahi S. A new correlation for estimating thermal conductivity of pure ionic liquids. *Fluid Phase Equilib.* 2013;354:199–206. <https://doi.org/10.1016/j.fluid.2013.06.004>.
  70. Ramires MLV, Nieto de Castro CA, Nagasaka Y. Standard reference data for the thermal conductivity of water. *J Phys Chem Ref Data.* 1995;24:1377–81.
  71. Jacquemin J, Husson P, Padua AAH, Majer V. Density and viscosity of several pure and water-saturated ionic liquids. *Green Chem.* 2006;8:172. <https://doi.org/10.1039/b513231b>.
  72. Tokuda H, Hayamizu K, Ishii K, Bin A, Susan H, Watanabe M. Physicochemical properties and structures of room temperature ionic liquids 2 variation of alkyl chain length in imidazolium cation. *J Phys Chem B.* 2005;109:6103–10. <https://doi.org/10.1021/jp044626d>.
  73. Chagnes A, Tougui A, Carré B, Ranganathan N, Lemordant D. Abnormal temperature dependence of the viscosity of ethylammonium nitrate-methanol ionic mixtures. *J Solut Chem.* 2004;33:247–55. <https://doi.org/10.1023/B:JOSL.0000035358.63305.b2>.
  74. Kundu N, Roy A, Dutta R, Sarkar N. Translational and rotational diffusion of two differently charged solutes in ethylammonium nitrate-methanol mixture: does the nanostructure of the amphiphiles influence the motion of the solute? *J Phys Chem B.* 2016;120:5481–90. <https://doi.org/10.1021/acs.jpcc.6b02251>.
  75. Stettner T, Gehrke S, Ray P, Kirchner B, Balducci A. Water in protic ionic liquids: properties and use of a new class of electrolytes for energy-storage devices. *Chemsuschem.* 2019;12:3827–36. <https://doi.org/10.1002/cssc.201901283>.

**Publisher's Note** Springer Nature remains neutral with regard to jurisdictional claims in published maps and institutional affiliations.